Optics Letters

Perfectly absorbing ultra thin interference coatings for hydrogen sensing

Murat Serhatlioglu,[1] Sencer Ayas,[1] Necmi Biyikli,[1] Aykutlu Dana,[1] and Mehmet E. Solmaz[2,*]

[1]Institute of Materials Science and Nanotechnology (UNAM), Bilkent University, Ankara 06800, Turkey
[2]Electrical and Electronics Engineering Department, Izmir Katip Celebi University, Izmir 35620, Turkey
*Corresponding author: mehmete.solmaz@ikc.edu.tr

Received 4 February 2016; revised 6 March 2016; accepted 8 March 2016; posted 9 March 2016 (Doc. ID 258841); published 5 April 2016

Here we numerically demonstrate a straightforward method for optical detection of hydrogen gas by means of absorption reduction and colorimetric indication. A perfectly absorbing metal-insulator-metal (MIM) thin film interference structure is constructed using a silver metal back reflector, silicon dioxide insulator, and palladium as the upper metal layer and hydrogen catalyst. The thickness of silicon dioxide allows the maximizing of the electric field intensity at the Air/SiO_2 interface at the quarter wavelengths and enabling perfect absorption with the help of highly absorptive palladium thin film (~7 nm). While the exposure of the MIM structure to H_2 moderately increases reflection, the relative intensity contrast due to formation of metal hydride is extensive. By modifying the insulator film thickness and hence the spectral absorption, the color is tuned and eye-visible results are obtained.

OCIS codes: (310.1620) Interference coatings; (310.6188) Spectral properties; (280.4788) Optical sensing and sensors; (260.3910) Metal optics.

http://dx.doi.org/10.1364/OL.41.001724

Hydrogen (H_2) sensing requires development of highly sensitive, reliable, and short response-time sensors due to its use in critical applications such as fuel-cells, pharmaceuticals, and petroleum and chemical production. Palladium (Pd) can absorb H_2 upon exposure and transform into palladium hydride (PdH_x), and the optical and electrical properties of Pd metal are changed by such transformation [1]. Recent advancements in plasmonic research and nanofabrication techniques led the development of surface and localized surface plasmon-based (LSPR) hydrogen sensors using Pd [2–4]. Nanoparticle or LSPR sensors show good potential for faster response times [5,6]. However, the broad spectral response of LSPR-based hydrogen sensors arises as an issue, which, later on, led the researchers to reduce the linewidth with the help of a whispering gallery mode cavity [7], and to develop highly sensitive hybrid sensors such as using Pd with a good plasmonic metal [8,9]. For example, Alivisatos and co-workers have demonstrated highly sensitive hydrogen sensors by placing Pd nanoparticles close to the sharp corners of nanoantennas [10]. Such sensing mechanisms are based on probing of the scattering properties of nanoantenna-Pd nanoparticle structure, rather than the direct probing of scattering properties of Pd nanoparticles that shows small wavelength shifts upon hydrogen exposure. Other important plasmon-based hydrogen sensing mechanism is based on plasmonic-perfect absorbers [11–13], and single crystal Pd and its alloy-coated nanowires [14,15]. The motivation behind the absorbance-based sensors is to minimize the requirement for the bulky optical setups, expensive light sources, and spectrometers by only probing the scattered light intensity at perfect-absorption wavelength. Moreover, some of the recent studies report the visual detection of hydrogen by using thin film optical coatings to circumvent the problems of hydrogen sensors based on electrical readout [16,17]. Despite the demonstration of visual detection of H_2, the thin film structure did not take full advantage of the lossy nature of Pd films. In this study, we demonstrate a nonplasmonic hydrogen gas sensor scheme based on perfectly absorbing thin film interference coatings with metallic mirror/insulator/Pd layers. Perfect absorption is obtained by the top ultra-thin Pd layer. The same scheme also allows the colorimetric detection of hydrogen gas. Such perfect absorber geometry offers cheap, eye-visible, and potentially highly sensitive hydrogen sensors with faster response times.

Thin film metal-insulator-metal (MIM) structures with different metals are studied in the literature to increase absorption in the visible and IR wavelengths for optical filtering and structural coloring applications [18,19]. Although the quality factors of these surfaces are comparable with the plasmonic grating surfaces, these surfaces are not suitable for sensing applications due to the highly confined nature of light into the dielectric layer. Yet, the optical properties of top metal can be altered by external stimuli to tune the resonance wavelength, which is essential for hydrogen sensing applications. The schematic of a 3-layer MIM structure with the substrate (Si) is given in Fig. 1(a). The proposed sensing mechanism in this Letter is due to the transformation of Pd layer to PdH_x via exposure to H_2, which also results in color change of the whole surface in room temperature. SiO_2 is a lossless and transparent insulator substrate with almost all the light falling on the thick Ag layer being reflected. With the top Pd layer, the spectral reflectance is around 90% beyond 400 nm wavelength [Fig. 1(b)]. When Ag

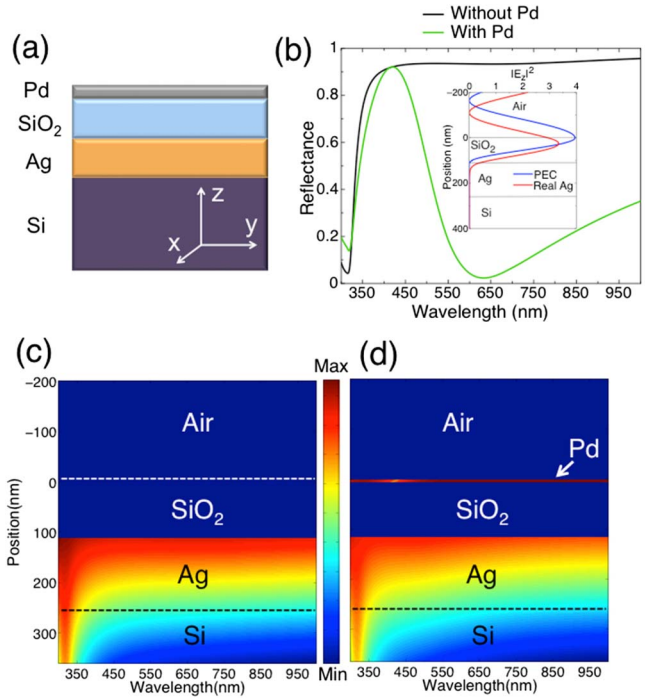

Fig. 1. (a) Schematic of a 3-layer system on Si substrate; (b) the reflectance spectra of the MIM structure with and without 5 nm Pd on SiO_2 showing transition to near-perfect absorption around 634 nm. The inset shows the E-field intensity when Ag is treated as perfect electric conductor (PEC) and a real metal with finite constants; (c) absorbed power distribution in logarithmic scale without Pd layer as a function of wavelength; (d) absorbed power distribution with peak absorption and 94% of the optical power is inside the ultra-thin Pd layer.

is assumed a perfect electric conductor (PEC), the quarter-wavelength thick (110 nm) SiO_2 layer allows the excitation of fundamental interference mode at $\lambda \cong 660$ nm with $n_{SiO2} = 1.5$ and the electric field enhancement is maximized at the Air/SiO_2 interface [Fig. 1(b), inset]. However, due to the finite optical constants of Ag [20], the field enhancement shifts to longer wavelengths and the highest field intensity is inside the insulator section for $\lambda \cong 660$ nm. When a thin absorbing film is placed on top of SiO_2, the reflectance of the system is expected to decrease [21]. Because Pd has large absorption in the visible wavelengths due to interband transitions [22], depositing thin Pd films results in near perfect absorption (97.7%) around the resonance wavelength of 634 nm. The optimum Pd thickness to achieve perfect absorption will be discussed later. To see the effect of 5 nm Pd layer on the optical absorption properties of the 3-layer MIM structure, we calculated the absorbed power distribution with and without Pd for the wavelength spectrum using transfer matrix method. Most of the optical power is absorbed in Ag and the absorption peak is at the SiO_2/Ag interface for the 2-layer system [Fig. 1(c)]. Five nanometer Pd film on a SiO_2 absorbs 94% of the optical power and 3.5% is absorbed by Ag [Fig. 1(d)]. Unlike nanostructured plasmonic absorber surfaces, the 3-layer MIM system presents near-perfect absorption without the requirement for any nanopatterning [10,11].

With H_2 absorption, the lattice parameters and the relative permittivity of Pd metal change. Here we ignore the volume expansion resulting from lattice constant increase [23]. In order to examine the difference in reflectance the transformation to PdH_x makes, we obtained dielectric function values of Pd and PdH_x reported by Vargas *et al.* [24] for 0.82 hydrogen concentration, and computed the absorptive characteristics of 3-layer MIM system for normal incidence where P dH_x is in β-phase ($x = 0.82$) [4]. It should also be noted that both the real and imaginary parts of the refractive index decreases with increasing H_2 concentration, and thus the results should be adjusted accordingly. With SiO_2 and Ag thicknesses fixed at 90 nm and 150 nm, respectively, we calculated and plotted the relative intensity contrast, RIC $= (R_{PdH_x} - R_{Pd})/R_{Pd}$, in logarithmic scale [Fig. 2(a)] as a function of Pd and PdH_x thickness where R_{Pd} and R_{PdH_x} are the reflection spectra before and after the H_2 exposure. For the selected SiO_2 and Ag thicknesses, the maximum RIC increase is localized around 500 nm. The spectral location of the reflectance minimum can be tuned by varying the SiO_2 thickness; thicker SiO_2 results in a red shift while thinner SiO_2 shifts the location to lower wavelengths. More discussion on this topic will be done later in the manuscript. The optimum Pd thickness for perfect absorption is around 7 nm and changes minimally along the spectrum with changing the SiO_2 thickness. The ultra-thin nature of the Pd metal allows faster H_2 uptake and more sensitivity in a sensing environment [25,26]. When the Pd is 7 nm, the reflection coefficient at the resonance wavelength ($\lambda \sim 518$ nm) becomes $\sim 3 \times 10^{-6}$ to achieve perfect absorption, and the largest RIC value obtained at ~518 nm is 2.93×10^4 [Fig. 2(b)] with perfect absorption decreasing. The resonance wavelength redshifts with increasing SiO_2 thickness. Because the value of RIC is

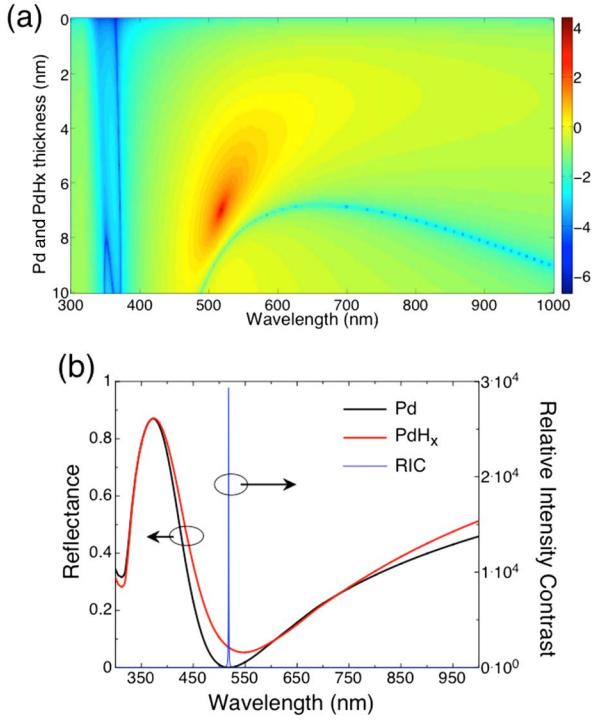

Fig. 2. Effect of Pd layer thickness on the reflection spectrum of MIM absorber. (a) Logarithmic 3D *RIC* spectrum with 7 nm Pd and PdH_x and 90 nm SiO_2 on 150 nm Ag; (b) 2D reflectance with and without H_2 exposure and the spectral location of maximum RIC is around 518 nm.

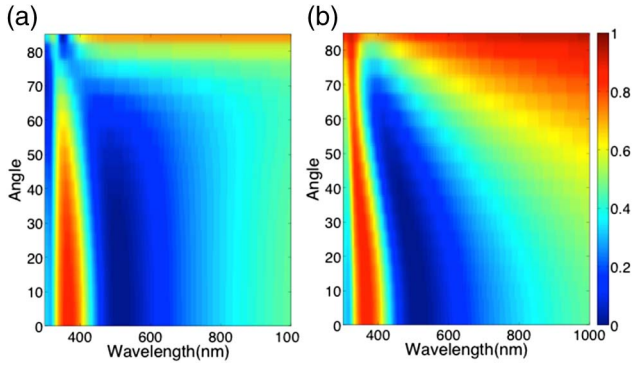

Fig. 3. Angle dependent reflectance (a) TM and (b) TE polarizations. 7 nm Pd and 90 nm SiO_2 is on top of the Ag reflector layer.

quite large for our MIM device, it can be considered as a great potential for a nonplasmonic hydrogen-sensing device. Such device's geometry can simplify sensor technology by illuminating the surface with a narrow band light source around the perfect absorption wavelength and detecting the reflected light by a detector.

The reflectance of the proposed 3-layer MIM structure was investigated in terms of angle dependence. The angle of incoming light rays was changed between 0° and 85° and the reflectance values for unexposed Pd were recorded for transverse-magnetic (TM) polarization [Fig. 3(a)]. The thickness values for Pd and SiO_2 are 7 nm and 90 nm, respectively. The 3-layer thin film interference structure shows angle-independence until 55° oblique incidence. The same computation was performed for transverse-electric (TE) polarization [Fig. 3(b)] to model the polarization dependence. TE polarization shows more angle dependence due to more phase mismatch for the same material thicknesses. Electric field components of TM and TE polarizations are parallel and normal to the surface of incidence, respectively. Hence, their angle-dependent reflectance properties are different from each other. Both polarization states show angle dependence at high oblique incidences. These results suggest that TM polarization is more suitable for absorption-based sensor scheme.

In order to predict the surface color of the 3-layer MIM system and graphically represent the chromaticity of colors, we looked at the CIE 1931 color space created by the International Commission on Illumination. The MIM structure produces subtractive colors in visible domain by rejecting certain wavelengths. Therefore, depending on the distribution of light intensity over the reflectance spectra, the surface color will be altered. The visual color of the surface can be found by integrating the multiplication of the spectrum of the light (i.e., radiance) with the spectral reflection of the surface at each wavelength and incorporating color matching functions [27–29]. The reflectance spectra of the MIM structures with 7 nm Pd and PdH_x on 80, 90, and 100 nm SiO_2 were calculated [Fig. 4(a)], where the resonance wavelengths for these thicknesses are in the visible wavelengths and exhibit a distinct surface color. Because the visual color of the 3-layer MIM system depends on the illuminating light source, we tried two different sources to predict the surface color: (a) a black body radiation source with effective temperature of 5800 K mimicking the solar spectrum; and (b) a white-light LED from a

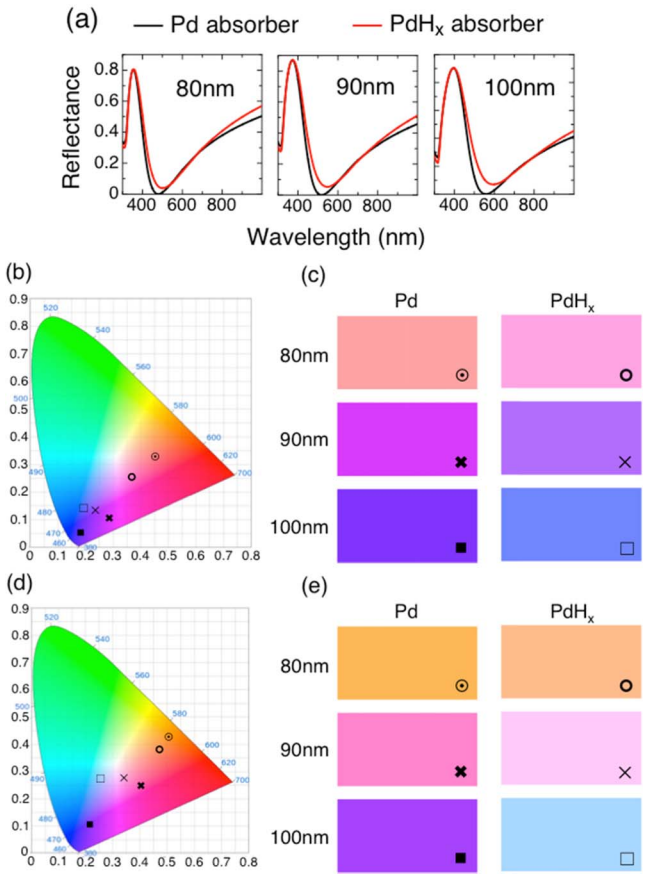

Fig. 4. Colorimetric sensing performances of MIM absorbers with different SiO_2 thicknesses. (a) Spectral reflectance of Pd and PdH_x 3-layer structure with different SiO_2 thicknesses; (b) CIE chromaticity diagram for reflectance of the MIM structures at normal incidence for 5800 K black body radiation; (c) the predicted surface color change resulting from H_2 exposure; (d) chromaticity diagram for white LED; (e) the predicted surface color change resulting from H_2 exposure differs from the results in (c).

cell-phone. The spectral radiance of the black body source was calculated using Planck's law, while the spectrum of the white-light LED of a Samsung cell-phone was measured using an Ocean Optics spectrometer. Then the CIE chromaticity coordinates of the reflective surfaces were calculated using a Matlab script. CIE 1931 color space chromaticity diagram of black body irradiated surface is given in Fig. 4(b), and the locations of the RGB color coordinates of MIM structures are labeled. All three MIM structures with different SiO_2 thicknesses show an obvious color change with Pd transformation to PdH_x via H_2 exposure [Fig. 4(c)]. The chromaticity diagram of the white-light LED irradiated surface differs moderately from the black body irradiated surface [Fig. 4(d)]. The color changes of the different MIM structures due to PdH_x transformation are also visually clear [Fig. 4(e)]. It is important to note that although the color coordinates remain the same, the predicted color may differ based on the computer monitor used. However, this does not affect the color change.

In conclusion, we presented a thin-film interference MIM structure based on ultra-thin Pd metal toward a cheap, sensitive, and eye-visible H_2 sensing scheme. The MIM structure

achieves near-perfect absorbance at visible wavelengths. Upon H_2 exposure, the reflectance increases due to PdH_x formation and a substantial relative intensity contrast is achieved, which allows absorption based H_2 detection. The location of reflectance minimum can be tuned controlling the lateral geometry of SiO_2. Because reflectance spectra of a 3-layer system has a single resonance and mimics a subtractive (bandreject) optical filter, the color change produced by H_2 exposure was investigated. CIE 1931 xyz chromaticity coordinates are found and eye-visible color change are simulated for two different illumination sources. The proposed H_2 sensing scheme offers a straightforward and relatively cheap fabrication process without any lithography steps. Due to the ultra-thin Pd layer, these thin film interference surfaces might pave the way for optical sensors with faster H_2 sensing kinetics in room temperature.

Funding. The Scientific and Technological Research Council of Turkey (TUBITAK) (111M344).

Acknowledgment. The authors thank Osman Balci and Nurbek Kakenov for useful discussions.

REFERENCES

1. R. B. Gupta, *Hydrogen Fuel: Production, Transport, and Storage* (CRC Press, 2008).
2. C. Wadell, S. Syrenova, and C. Langhammer, ACS Nano **8**, 11925 (2014).
3. K. Lin, Y. Lu, J. Chen, R. Zheng, P. Wang, and H. Ming, Opt. Express **16**, 18599 (2008).
4. C. Langhammer, I. Zoric, B. Kasemo, and B. M. Clemens, Nano Lett. **7**, 3122 (2007).
5. A. Tittl, X. Yin, H. Giessen, X.-D. Tian, Z.-Q. Tian, C. Kremers, D. N. Chigrin, and N. Liu, Nano Lett. **13**, 1816 (2013).
6. J. M. Bingham, J. N. Anker, L. E. Kreno, and R. P. Van Duyne, J. Am. Chem. Soc. **132**, 17358 (2010).
7. F. Gu, L. Zhang, Y. Zhu, and H. Zeng, Laser Photon. Rev. **9**, 682 (2015).
8. A. Dasgupta and G. Kumar, Appl. Opt. **51**, 1688 (2012).
9. A. Tittl, C. Kremers, J. Dorfmüller, D. N. Chigrin, and H. Giessen, Opt. Mater. Express **2**, 111 (2012).
10. N. Liu, M. L. Tang, M. Hentschel, H. Giessen, and A. P. Alivisatos, Nat. Mater. **10**, 631 (2011).
11. A. Tittl, P. Mai, R. Taubert, D. Dregely, N. Liu, and H. Giessen, Nano Lett. **11**, 4366 (2011).
12. N. Liu, M. Mesch, T. Weiss, M. Hentschel, and H. Giessen, Nano Lett. **10**, 2342 (2010).
13. C. Hu, Z. Zhao, X. Chen, and X. Luo, Opt. Express **17**, 11039 (2009).
14. F. Gu, H. Zeng, L. Tong, and S. Zhuang, Opt. Lett. **38**, 1826 (2013).
15. F. Gu, H. Zeng, Y. Zhu, Q. Yang, L. Ang, and S. Zhuang, Adv. Opt. Mater. **2**, 189 (2014).
16. P. Ngene, T. Radeva, M. Slaman, R. J. Westerwaal, H. Schreuders, and B. Dam, Adv. Funct. Mater. **24**, 2374 (2014).
17. M. E. Nasir, W. Dickson, G. A. Wurtz, W. P. Wardley, and A. V. Zayats, Adv. Mater. **26**, 3532 (2014).
18. Z. Li, S. Butun, and K. Aydin, ACS Photon. **2**, 183 (2015).
19. K. T. Lee, S. Seo, and L. J. Guo, Adv. Opt. Mater. **3**, 347 (2015).
20. A. D. Rakić, A. B. Djurišić, J. M. Elazar, and M. L. Majewski, Appl. Opt. **37**, 5271 (1998).
21. Z. Li, E. Palacios, S. Butun, H. Kocer, and K. Aydin, Sci. Rep. **5**, 15137 (2015).
22. T. Pakizeh, C. Langhammer, I. Zoric, P. Apell, and M. Käll, Nano Lett. **9**, 882 (2009).
23. T. B. Flanagan and W. Oates, Annu. Rev. Mater. Sci. **21**, 269 (1991).
24. W. Vargas, I. Rojas, D. Azofeifa, and N. Clark, Thin Solid Films **496**, 189 (2006).
25. P. Soundarrajan and F. Schweighardt, *Hydrogen Fuel: Production, Transport, and Storage*, R. B. Gupta, ed. (CRC Press, 2008), pp. 495–534.
26. F. Yang, S.-C. Kung, M. Cheng, J. C. Hemminger, and R. M. Penner, ACS Nano **4**, 5233 (2010).
27. P. Martin, *Introduction to Surface Engineering and Functionally Engineered Materials* (Wiley, 2011), Vol. **74**.
28. R. J. H. Ng, X. M. Goh, and J. K. W. Yang, Opt. Express **23**, 32597 (2015).
29. J. Schanda, *Colorimetry: Understanding the CIE System* (Wiley, 2007).